communications biology

A Nature Portfolio journal

Article

https://doi.org/10.1038/s42003-025-08871-6

Spatially global effects of feature-based attention in functional subdivisions of human subcortical nuclei

Weiru Lin[1,2,10], Chencan Qian[1,2,10], Yan-Yu Zhang[3], Shang Liu[1,2], Xilin Zhang[4,5], Fang Fang[6,7,8,9] & Peng Zhang[1,2]

Attention can prioritize the processing of non-spatial features throughout the visual field, yet the neural mechanisms of feature-based attention in subcortical regions remain poorly understood. Using high-resolution functional magnetic resonance imaging (fMRI) at 7 T, we investigated the global effects of color-based attention in functional subdivisions of human subcortical nuclei. Color-based attention selectively enhanced activity in the parvocellular layers of the lateral geniculate nucleus of the thalamus for unattended stimuli across the visual field, while reducing responses to attended stimuli. Both feedforward and feedback connectivity with the primary visual cortex were enhanced. In addition, our results suggest that the deeper layers of the superior colliculus contribute to attentional control of this spatially global effect, while the ventral pulvinar coordinates connectivity between visual areas. Together, these findings uncover a global attention mechanism in the visual thalamus and reveal the distinct roles of subcortical nuclei in feature-based attention.

Selective attention allows our brain to process behaviorally relevant information in cluttered visual scenes. Attention can be directed to spatial locations, or to non-spatial features such as color or motion direction. In feature-based attention, items that shared the same feature as the attended target can be prioritized throughout the visual field, independent of the spatial location of the visual items[1–3]. While the neural mechanisms of spatial attention have been extensively studied in both cortical and subcortical regions[4,5], much less is known about the neural mechanisms of feature-based attention, especially in subcortical regions.

Paying attention to the non-spatial feature of a stimulus selectively activates the sensory cortex specialized for processing the attended feature dimension, such as the motion-sensitive area MT or color-sensitive area V4[6,7]. Within these brain regions, neuronal activity is either enhanced or suppressed depending on the similarity between the attended feature value and the neuronal feature tuning, even when the receptive field of the neuron is located far outside the focus of spatial attention[8,9]. The spatially global effect of feature-based attention has also been demonstrated in neuroimaging studies[10–13], further supporting the feature-similarity gain model of attention[8]. Beyond the visual cortex, attended features can be decoded from multivoxel patterns in the frontoparietal regions[14]. Causal evidence from an electrophysiological study in monkeys[15] and effective fMRI connectivity in humans[13] support the prefrontal cortex as a source for controlling feature-based attention. However, a recent study showed that the attentional gain modulation of PFC neurons is independent of the feature tuning of neurons in a feature-based attention task[16]. Thus, the neural mechanisms of feature-based attention in the frontoparietal cortex remain unclear.

In subcortical regions, neural mechanisms of spatial attention have been well studied in the lateral geniculate nucleus (LGN), thalamic reticulate nucleus (TRN), and pulvinar of the thalamus[17–19], and in the superior colliculus (SC) of the brainstem[20]. LGN activity can be strongly modulated by top-down spatial attention[21–23], with early modulation by the TRN and late modulation likely through cortical feedbacks[23,24]. The pulvinar plays a critical role in the control of spatial attention[25] and regulates information

[1]State Key Laboratory of Cognitive Science and Mental Health, Institute of Biophysics, Chinese Academy of Sciences, Beijing, China. [2]University of Chinese Academy of Sciences, Beijing, China. [3]School of Psychology, Shanghai Jiao Tong University, Shanghai, China. [4]Key Laboratory of Brain, Cognition and Education Sciences, Ministry of Education, South China Normal University, Guangzhou, Guangdong, China. [5]School of Psychology, Center for Studies of Psychological Application, and Guangdong Provincial Key Laboratory of Mental Health and Cognitive Science, South China Normal University, Guangzhou, Guangdong, China. [6]School of Psychological and Cognitive Sciences and Beijing Key Laboratory of Behavior and Mental Health, Peking University, Beijing, China. [7]IDG/McGovern Institute for Brain Research, Peking University, Beijing, China. [8]Peking-Tsinghua Center for Life Sciences, Peking University, Beijing, China. [9]Key Laboratory of Machine Perception (Ministry of Education), Peking University, Beijing, China. [10]These authors contributed equally: Weiru Lin, Chencan Qian.
e-mail: zhangpeng@ibp.ac.cn

transmission between cortical areas at the attended location[19,26]. The superficial and deeper layers of the SC have been proposed to encode the saliency and priority maps of attention, respectively[27–29]. While much evidence supports the important roles of these subcortical nuclei in spatial attention, little is known about the subcortical mechanisms underlying feature-based attention. The only human fMRI study about feature-based attention showed stronger BOLD signals in the LGN and pulvinar when participants attended to motion compared to color in spatially overlapping fields of moving and colored dots[30]. However, the spatially global effect of feature-based attention in functional subdivisions of the subcortical nuclei has not been convincingly demonstrated.

After the retina, the LGN is the earliest stage of the visual pathway that processes feature-selective information. It consists of two magnocellular (M) layers and four parvocellular (P) layers in the ventral and dorsal subdivisions of the nucleus, respectively. Neurons in the P layers prefer color, high spatial frequency, and low temporal frequency stimuli, whereas neurons in the M layers are sensitive to motion, and luminance contrast stimuli at low spatial frequency and high temporal frequency[31,32]. Feature-selective neurons have also been found in the pulvinar[33,34], which consists of several functional subdivisions with distinct connectivity patterns with cortical regions. The ventrolateral pulvinar (vlPul) is interconnected with the early visual cortex and the ventral visual stream, whereas the ventromedial pulvinar (vmPul) receives projection from the SC and connects to the dorsal visual stream[35–37].

Therefore, it is possible that feature-based attention could modulate feature-selective processing in functional subdivisions of the visual thalamus, controlled by cortical and subcortical attention network regions. Recent studies showed that high-resolution fMRI is capable to resolve fine-scale activity in functional subdivisions of human subcortical nuclei[38–42]. Thus, to investigate the neural mechanism of feature-based attention in human subcortex and its relationship with cortical regions, we used high-resolution fMRI (1.5-mm isotropic voxels) at 7 Tesla to investigate the spatially global effects of color-based attention in the functional subdivisions of human subcortical visual nuclei (i.e., LGN, Pulvinar, and SC), early visual cortices, and frontoparietal attention networks.

Results

We carefully calibrated visual stimuli to isolate L/M cone opponent color processing in the early visual areas, particularly the P layers of the LGN[32]. In the behavioral experiment, we investigated whether paying attention to the same compared to different colors across the visual field could improve color discrimination performance in dual tasks[43]. In the fMRI experiments, we investigated whether the attended color matching the color of the unattended stimulus across the visual field could significantly modulate BOLD signals in the brain regions of interest (Experiment 1, Exp. 1), and whether the attended color could be decoded from brain activity to spatially overlapping red/green stimuli presented at attended and unattended locations (Experiment 2, Exp. 2).

Attention to the same color in both hemifields improves color discrimination performance in dual tasks

In the behavioral experiment (Fig. 1a), participants performed two color discrimination tasks simultaneously at two different locations across the visual field. At the beginning of each trial, two colored dots next to the fixation point indicated the colors of the target dots to be attended. After pressing a button, two spatially overlapping fields of red and green dots were presented on each side of fixation in two 1000-ms intervals, separated by a 100-ms fixation period. Participants paid attention to the cued dots, and responded in which interval the stimulus appeared more saturated. Feedback was given after responses. The result showed significantly better performance when the attended colors were the same compared to different across the visual field (Fig. 1b, $t(24) = 9.425$, $P < 0.001$, Cohen's $d = 1.202$). This replicates the previous findings by Saenz and colleagues[43]. The results are consistent with a spatially global effect of feature-based attention: paying attention to a stimulus feature facilitates the processing of multiple stimuli sharing the same feature across the visual field. The same-color benefit may reflect reduced switching costs when attention is focused on a single feature value[44].

Color similarity between attended and unattended stimuli across the visual field selectively modulates P layer activity in the LGN

In the fMRI session, isoluminant L-M cone-contrast defined red/green disk flickers were used as a chromatic functional localizer to selectively activate the P layers of the LGN (Fig. 1c). In Exp. 1 (Fig. 1d), participants were instructed to discriminate in which interval the attended color appear more saturated, while ignoring the colored dots on the opposite side of fixation. The ignored dot fields were presented in either the same or a different color than the attended dots. Behavioral performance did not show a significant difference between the same (mean ± std: 73.48% ± 8.75%) and different (73.44% ± 9.44%) conditions ($t(24) = 0.030$, $P = 0.976$, $BF_{10} = 0.211$). In Exp. 2 (Fig. 1e), spatially overlapping red and green dots were presented in both attended and unattended visual fields. Participants performed the same task as in Exp. 1 (71.42% ± 8.66%).

The anatomically delineated LGN mask was divided into M and P subdivisions based on the ventromedial-to-dorsolateral laminar organization of the human LGN, at a volume ratio of 1:4 (Fig. 2a and Supplementary Fig. S1)[45]. Supplementary Fig. S2 shows the LGN ROIs for all individuals. The chromatic localizer activated the P subdivision in the dorsolateral LGN (Fig. 2b), whereas the colored moving dots presented on a black background strongly activated both P and M subdivisions (Fig. 2c, d). Figure 2c shows the activation maps in Exp. 1 when the attended color and the color of the unattended stimulus in the opposite visual field were the same or different, and the response difference between the two conditions. The differential map between the same and different conditions shows a stronger activation in the P subdivisions of the LGN contralateral to the unattended visual field.

To further investigate the spatially global effects of color-based attention in Exp. 1, we analyzed the ROI-averaged BOLD response to visually responsive voxels in the M and P subdivisions. P-biased voxels (LGNp) were defined as those in the P subdivision with strong activations in the chromatic localizer, while M-biased voxels (LGNm) were defined as those in the M subdivision with strong activations to the moving dots against a black background in Exp. 2. The ROI-averaged BOLD timecourses in the contralateral LGNs clearly showed a transient response followed by a flat portion of sustained response (indicated by light and dark shaded areas in Fig. 2e, f, respectively). To avoid the non-specific transient signals due to changes in arousal and transient attention[46], we focused on the sustained response period in the following analysis (see Supplementary Fig. S3 for the results of the transient response). The time window of sustained response was defined from the "knee" point on the time course to the stimulus offset. A leave-one-subject-out procedure was used to determine the sustained response period (see "Methods").

The bar plots in Fig. 2e, f show the mean BOLD response in the sustained response period. Color-based attention exhibited distinct patterns of response modulation in the parvocellular and magnocellular subdivisions of the LGN (significant three-way interaction among layer (LGNp/LGNm), attention (attended/unattended), and similarity (same/different) in a repeated measures ANOVA, $F(1,24) = 5.934$, $P = 0.023$, $\eta_p^2 = 0.198$). Follow-up tests showed a significant global effect of feature-based attention in LGNp (similarity × attention interaction: $F(1,24) = 9.874$, $P = 0.004$, $\eta_p^2 = 0.291$), but not in LGNm ($F(1,24) = 0.001$, $P = 0.972$, $\eta_p^2 = 5.126\times10^{-5}$). In LGNp, the BOLD response to stimuli presented at the unattended location was significantly enhanced when its color matched the attended color ("same" condition, $t(24) = -2.663$, $P = 0.014$, Cohen's $d = 0.565$) compared to the "different" condition, while the BOLD response to stimuli presented at the attended location was significantly reduced ($t(24) = -2.153$, $P = 0.042$, Cohen's $d = 0.383$). The statistics in LGNp were robust to the number of voxels when defining the ROI (Supplementary Fig. S4). To minimize the influence of overall BOLD response difference on the modulation effect, we also calculated a color similarity modulation index as $(S - D)/\mathrm{sqrt}(S^2 + D^2)$ (Supplementary Fig. S5). The result was qualitatively similar; a significant

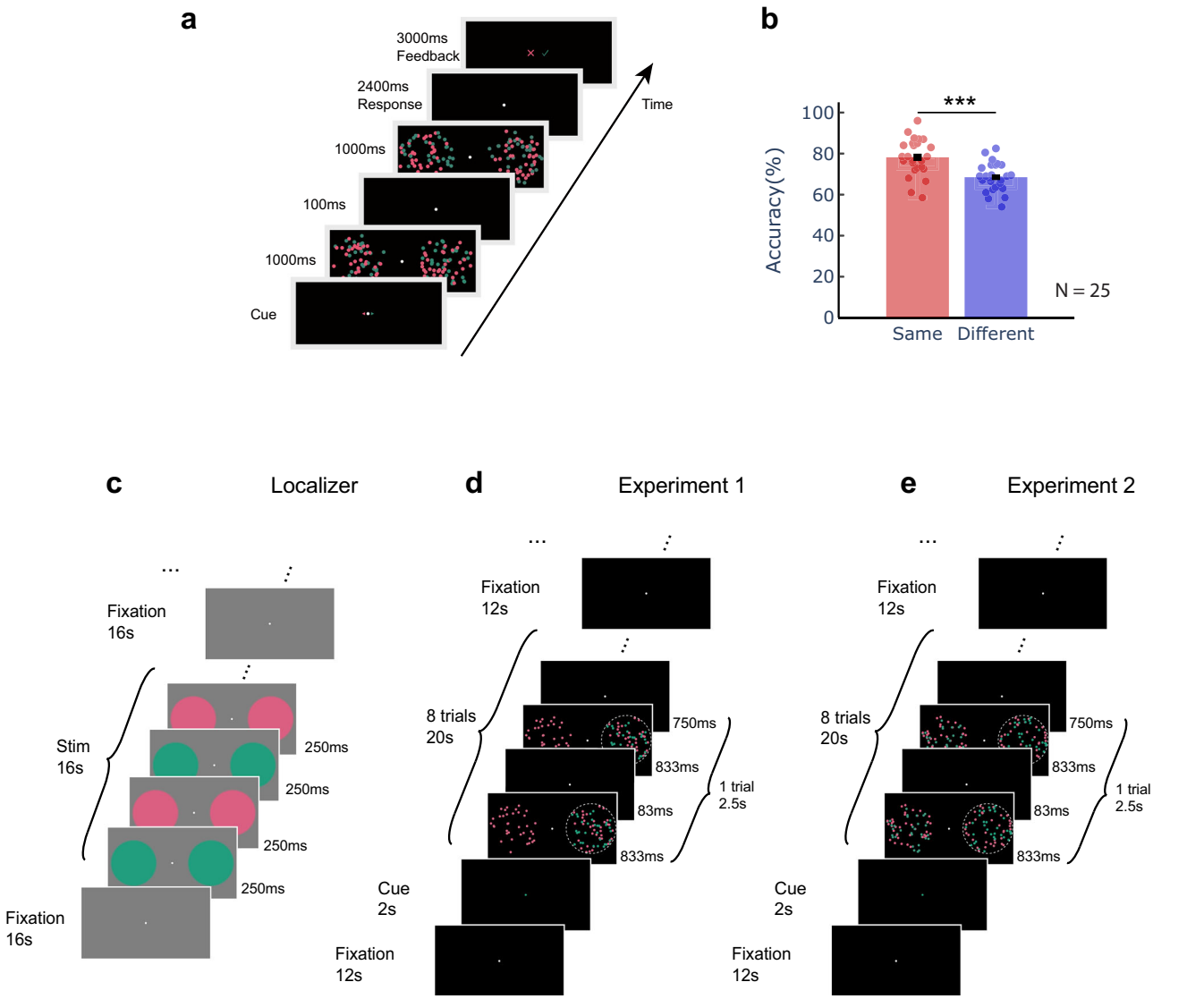

Fig. 1 | Schematic diagram of stimuli and procedures for the behavioral and fMRI experiments. a Stimuli and procedure for one trial in the behavioral experiment. **b** Color discrimination performance in behavioral experiment. **c** Stimuli and procedure for the functional localizer in the fMRI session. Uniform red and green disks in L-M cone contrast flickered at 2 Hz for 16 s, alternating with 16-s fixation on gray background. **d** Stimuli and procedure for Exp. 1. Participants attended to the cued dots at the cued location (indicated by the white dotted circle, which was not shown in the actual experiment), while ignoring the dots on the opposite side. In all, 20-s task blocks alternated with 12-s fixation periods. **e** Stimuli and procedure in Exp. 2 were the same as in Exp. 1, except that both red and green dots were presented at the unattended location. Error bars represent standard errors of the mean (SEM) across participants ($n = 25$).

color-similarity modulation was found in LGNp but not in LGNm. These findings clearly demonstrate that the similarity between the attended color and the color of unattended stimuli across the visual field significantly modulated BOLD responses in the P subdivision of the LGN. Our results cannot be explained by the difference in task difficulty between the same and different conditions, nor a "leakage" of spatial attention to the unattended side, since there was no significant difference in task performance ($t(24) = 0.030$, $P = 0.976$, $BF_{10} = 0.211$) or fixational eye movement (Supplementary Fig. S6), and the response reduction of attended stimuli in the "same" condition was only observed in LGNp, but not in the cortex (Fig. 5d, see below).

The spatially global effect of color-based attention in the LGN was further demonstrated by a multivoxel pattern analysis. Due to low signal-to-noise ratio in the subcortical regions and less anatomical and functional variability across participants, we normalized each subject's volumetric data in a standard space. A linear support vector machine (SVM) was trained to predict whether a trial was from the "same" or "different" condition, using a leave-one-subject-out cross-validation procedure (see "Methods"). The decoding accuracy for the LGN contralateral to the unattended stimuli was significantly above chance level (62%, $P < 0.001$, and $P = 0.006$ after correction for multiple comparison corrections across ROIs and attention conditions). Therefore, consistent with the univariate results, multivariate decoding shows that paying attention to a color matching the unattended stimuli across the visual field significantly modulated activity in the LGN contralateral to the unattended stimuli. Same vs. Diff pattern decoding was not significant in the SC and pulvinar, likely due to lower SNR in these regions.

Color similarity modulation of attention is significant in the deeper layers of the SC

The SC is a laminated nucleus on the brainstem that plays importation roles in the controls of attention and eye movements. Neurons in the superficial layers of the SC are visuosensory, while those in the deeper (intermediate and deep) layers are visuomotor and motor. Since the superficial layers are about 1/3 of the thickness of the primate SC[47], we generated a normalized depth map in the SC and divided it into superficial (SCs) and deeper (SCd)

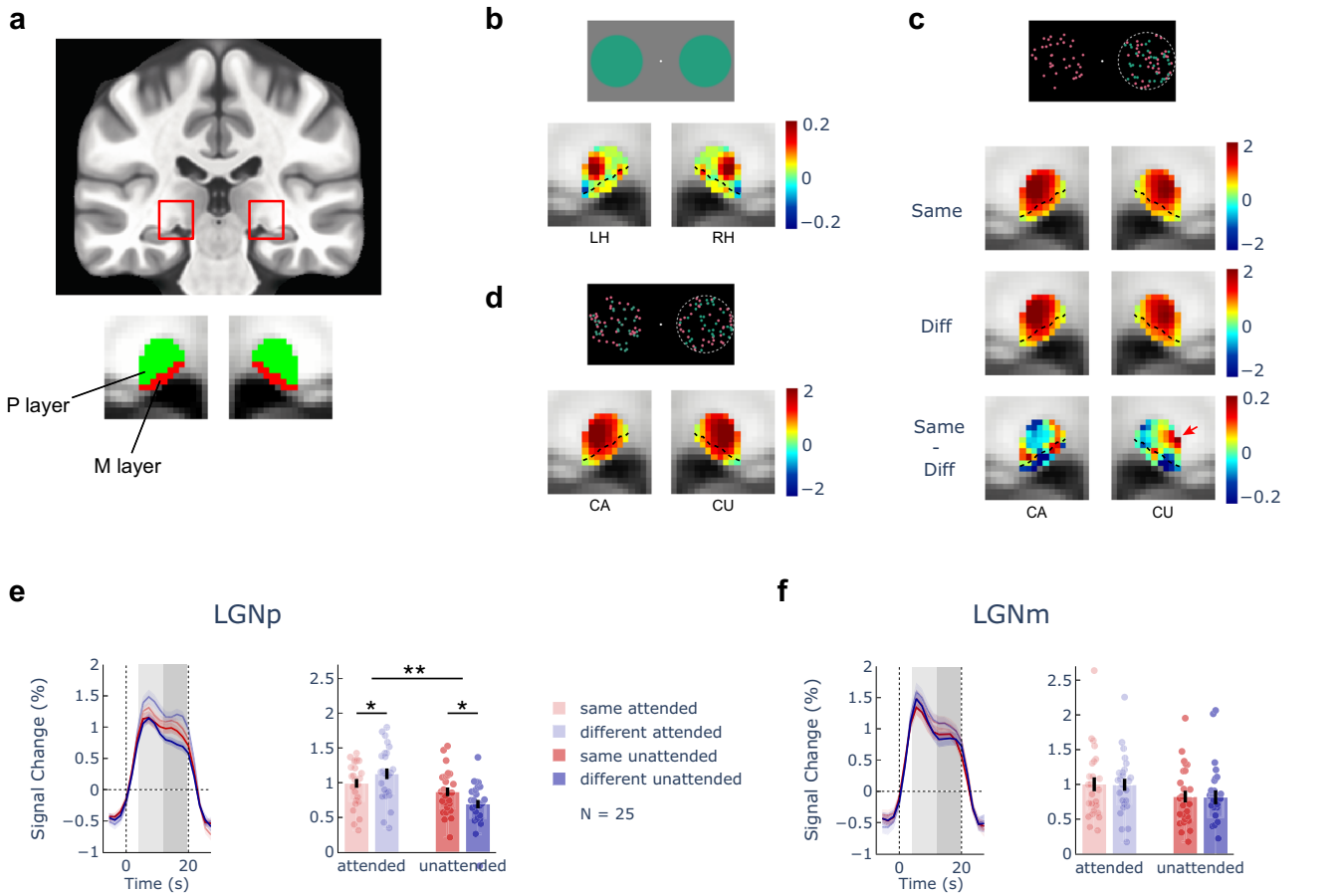

Fig. 2 | BOLD activation maps and ROI-averaged responses in functional subdivisions of the LGN. a The location of LGN in MNI space and the definition of M and P subdivisions in a coronal section. **b–d** show the activation maps to stimuli in the chromatic localizer, Exp. 1 and Exp. 2, respectively. The red arrow in (**c**) highlights the activation in the P subdivision to the spatially global effect of color-based attention. Color bars indicate the percent signal change of BOLD signals. LH left hemisphere, RH right hemisphere. CA, contralateral to the attended location. CU contralateral to the unattended location. **e**, **f** are ROI-averaged responses in LGNp and LGNm. Light and dark shaded areas in the time course plots indicate the transient and sustained response period, respectively. Shaded areas and error bars in the bar graph indicate SEM across participants ($n = 25$). $^{*}P < 0.05$, $^{**}P < 0.01$.

ROIs (Fig. 3a and Supplementary Fig. S7). Our results show that visual stimuli mainly activated SCs (Fig. 3b–d), which is consistent with the fact that neurons in the superficial layers mainly process visuosensory information. In Fig. 3c, there was a stronger activation in same compared to the different condition in the SC contralateral to the unattended visual field (same - diff, CU).

BOLD timecourses of the SC didn't show a distinction in transient and sustained responses (Fig. 3e, f), thus we averaged the response from 4 s after the stimulus onset to the stimulus offset for statistical analysis. Only SCd showed a significant color similarity modulation of attention (attention × similarity interaction: $F(1,24) = 7.753$, $P = 0.010$, $\eta_p^2 = 0.244$). An insignificant trend was found in SCs ($F(1,24) = 1.617$, $P = 0.216$, $\eta_p^2 = 0.063$). Given the important role of the deeper layers of the SC in attention control, our results suggest that they are involved in the control of the spatially global effect of feature-based attention.

Ventrolateral pulvinar shows a marginal effect of color similarity modulation of attention

The pulvinar is a large second-order thalamic nucleus that consists of several subregions with distinct functions and connectivity with cortical regions. According to a pulvinar atlas based on task co-activation patterns[48], we divided the posterior pulvinar into two ventral and two dorsal subregions (Fig. 4a and Supplementary Fig. S8). The ventrolateral (vlPul) and ventromedial (vmPul) pulvinar primarily connect with the ventral and dorsal visual streams[35], respectively, and selectively respond to parvocellular (P) and magnocellular (M) visual stimuli[49]. The dorsal subregions are more involved in higher-order cognitive functions and mainly connect with frontoparietal regions[50]. Since our stimuli mainly activated the ventral pulvinar (Fig. 4b–d), we focused our analyses on the two ventral subregions. From the activation map in Fig. 4c, the vlPul contralateral to the unattended visual field shows stronger activations in the same compared to the different condition. Like the LGN, the timecourses of ventral pulvinar showed a clear transient response followed by a sustained response (Fig. 4e, f). The sustained response period showed a trend of color-similarity modulation of attention (similarity × attention interaction: $F(1,24) = 3.387$, $P = 0.078$, $\eta_p^2 = 0.124$). A similar trend was also found for the transient response (Supplementary Fig. S3). However, the vmPul exhibited much weaker responses to our stimuli, with no significant effect of attention or color similarity. It suggests the need for a more precise atlas for the magnocellular portion of the ventral pulvinar.

Spatially global effects of color-based attention in early visual cortices and frontoparietal regions

Figure 5c shows the BOLD activation maps in cortical brain regions in Exp. 1. The early visual cortices and frontoparietal regions were activated in both the same (Fig. 5a) and different (Fig. 5b) conditions. The difference between the same and different conditions shows activations in V1, V4, and the posterior intraparietal sulcus (pIPS) in the hemisphere contralateral to the unattended stimuli. Cortical ROIs were defined by the functional localizer on the cortical surface (Supplementary Figs. S9 and S10). The ROI-averaged

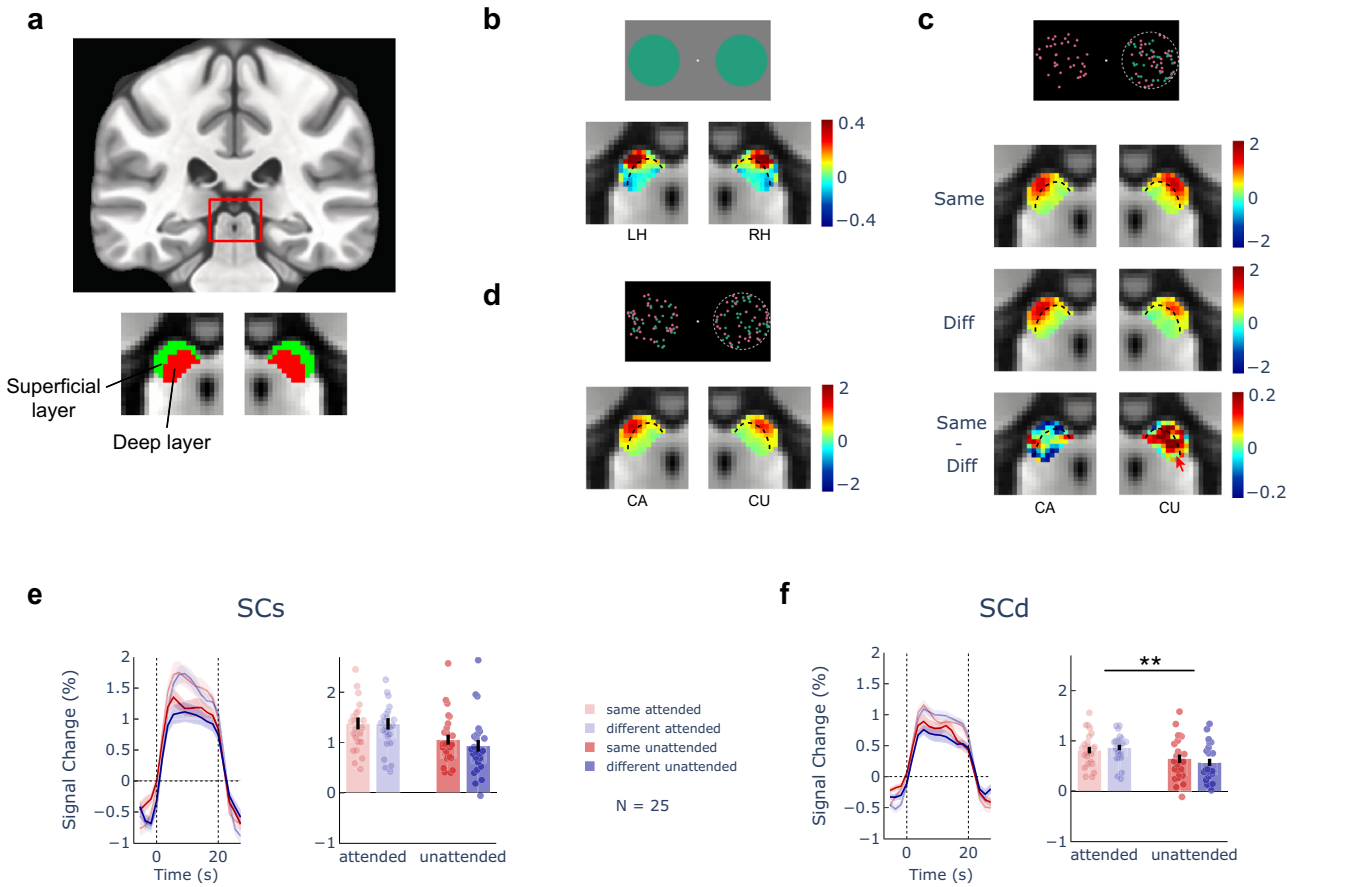

Fig. 3 | BOLD activation maps and ROI-averaged responses in the SC. a The location of SC in MNI space and the superficial and deeper layer ROIs. **b–d** are activation maps for chromatic localizer, Exp. 1, and Exp. 2, respectively. The red arrow in (**c**) highlights the activation to spatially global effect of color-based attention. Color bars indicate the BOLD response in percent signal change. LH left hemisphere, RH right hemisphere, CA contralateral to the attended side, CU contralateral to the unattended side. **e**, **f** are bar plots in the superficial and deep layers, respectively. Shaded areas and error bars indicate SEM across participants ($n = 25$). $^{**}P < 0.01$.

responses in Fig. 5d show significant global effects of color-based attention in the early visual cortices (V1–V4) and the pIPS. The timecourses for these cortical regions are shown in Supplementary Fig. S11. Consistent with previous studies[10,13], we found significantly stronger global effect of color attention in hV4 than in hMT+ (similarity × ROI interaction in the unattended condition: $F(1,24) = 23.858$, $P = 5.57 \times 10^{-5}$, $\eta_p^2 = 0.499$). These results support the spatially global effects of feature-based attention in the early visual cortices and the posterior parietal cortex.

Color-based attention modulates connectivity among cortical and subcortical regions

To further investigate how color-based attention modulates the information flow between cortical and subcortical regions, we used the dynamic causal modeling (DCM) to estimate the effective connectivity of fMRI signals among key brain regions as suggested by the previous analysis, including V1, V4, pIPS, LGN, SC, and vlPul. A full DCM model was defined based on the empirical evidence of anatomical connections among these regions[36,47,51,52]. In this model (Fig. 6a), the LGN receives the driving input; fixed or intrinsic connections were defined between and within brain regions; color similarity between the attended and unattended stimuli could modulate the effective connectivity in these connections, which were estimated separately in the attended and unattended conditions. At the first level, the full DCM model was estimated for the fMRI data within each hemisphere for each participant, and the results were averaged across the two hemispheres[53]. The second level of analysis used Bayesian model reduction, Bayesian model average, and parametric empirical Bayes to make inferences about the model evidence and connectivity strength[54].

Results of the second-level analysis are shown in Fig. 6b–d. Most of the fixed connections were highly significant (Fig. 6b), suggesting a good fit of the DCM model. In the attended hemisphere (hemisphere contralateral to the attended stimulus) (Fig. 6c), attended color similarity (same vs. diff) with the unattended stimulus significantly modulated the SC-LGN connectivity, and the connectivity between the pulvinar and early visual cortices. In the unattended hemisphere (hemisphere contralateral to the unattended stimulus) (Fig. 6d), color similarity with the attended stimulus significantly enhanced the feedforward and feedback connectivity between the LGN and V1. LGN activity was also modulated by the SC and pulvinar. The pIPS was suggested as a source of the top-down modulation. Like in the attended condition, color similarity enhanced the connectivity between the pulvinar and other visual areas, suggesting that the pulvinar was involved in coordinating the information transmission between visual areas in global feature-based attention.

Attended color can be decoded from multivoxel response patterns in the early visual cortices and frontoparietal regions

To further investigate whether the attended color can be decoded from brain activity to spatially overlapping red and green dots (from the attended location in Exp. 1 and Exp. 2, or from the unattended location in Exp. 2), we trained linear SVM classifiers with multi-voxel patterns of BOLD response in the hemisphere contralateral to the stimulus location. Results showed that in brain regions contralateral to the attended stimuli in Exp. 1 and Exp. 2 (Fig. 7, top panel, attended condition), the early visual cortices and frontoparietal regions showed significantly above chance decoding accuracy. In brain regions contralateral to the unattended stimuli in Exp. 2 (Fig. 7,

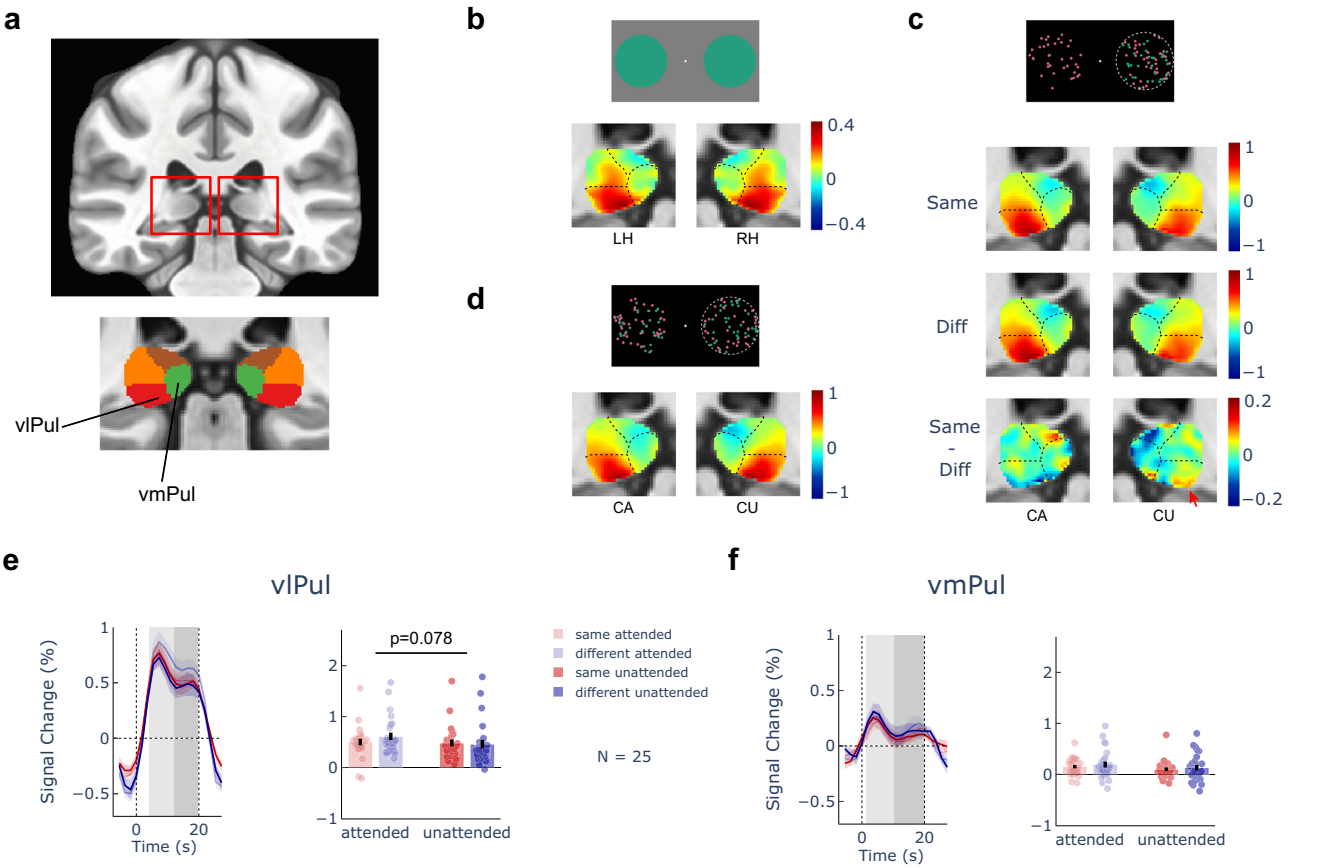

Fig. 4 | BOLD activation maps and ROI-averaged responses in the pulvinar. a The location of the pulvinar in MNI space and its subdivisions. **b–d** are activation maps for the chromatic localizer, Exp. 1, and Exp. 2, respectively. The red arrow in (**c**) highlights the activation to spatially global effect of color-based attention. Color bars indicate the BOLD response. LH left hemisphere, RH right hemisphere, CA contralateral to the attended side, CU contralateral to the unattended side. **e**, **f** show the ROI-averaged timecourses and bar plots in vlPul and vmPul. Light and dark shaded areas indicate the transient and sustained response period, respectively. Shaded areas and error bars represent SEM across participants ($n = 25$).

bottom, unattended condition), V2, V4, and IPS also showed significantly above-chance decoding performance, suggesting spatially global effects of feature-based attention across the visual field. The lower decoding accuracy in the unattended condition is due to less training data compared to the attended condition (4 vs. 8 runs). Decoding results with 4 runs of data in Exp. 2 shows similar performance as those in the unattended condition (Supplementary Fig. S12). For the subcortical ROIs, decoding performance was at chance level, likely due to the fine-scale organization of color-selective responses in subcortical nuclei, making it difficult to distinguish specific hues at the spatial resolution of our fMRI data. Stronger evidence for a spatially global effect in the subcortical ROIs would require decoding attended color information outside the stimulus region[11]. However, this is not possible in our data since decoding performance was at chance level even for the stimulus region. Consistent with the effective connectivity analysis, these findings support a source of the parietal cortex in controlling feature-based attention across the visual field.

No significant difference in fixation distribution between the same and different conditions

To determine whether the color similarity effect observed in the fMRI experiment was influenced by eye movements, we conducted an eye-tracking experiment outside the scanner in 6 out of the 20 participants while they performed the same task as in Exp. 1 of the fMRI session. As shown in Supplementary Fig. S6, the fixation distribution did not differ significantly between the same and different conditions, nor was there any systematic bias toward the attended or unattended side. Thus, the color similarity effect observed in the fMRI data was unlikely a result of eye movements artifact.

Discussion

Using high-resolution 7 T fMRI, we found spatially global effects of feature-based attention in functional subdivisions of human subcortical nuclei. When the color of an unattended stimulus across the visual field matched the attended color, BOLD signals in the P subdivision of the LGN were significantly enhanced for the unattended stimulus while reduced for the attended stimulus. The color similarity modulation of attention across the visual field was also found in the deeper layers of the SC. Both feedforward and feedback connectivity were enhanced between the LGN and V1. The SC and pulvinar were involved in top-down attentional modulation, with the pulvinar also coordinating the connectivity between visual areas. Finally, both effective connectivity and attended color decoding suggest a source of global feature-based attention from IPS of the parietal cortex.

In an electroencephalographic (EEG) study, the spatially global effect of feature-based attention was found to modulate the early P1 component of event-related potentials in the occipital lobe around 100 ms[12]. Our high-resolution fMRI results demonstrate that feature-based attention enhanced both feedforward and feedback processing of the attended feature information throughout the visual field in the LGN of the thalamus (Figs. 2c, e and 6d), which is the earliest stage of feature-selective processing after the retina. Furthermore, color similarity modulation was significant in P but not M layers of the LGN, suggesting a similarity-based modulation of early color-selective processing. While the Feature Similarity Gain Model was originally proposed based on direction-selective neurons in the magnocellular stream[8], our findings are conceptually consistent with its broader prediction that attention enhances responses to stimuli matching the attended feature.

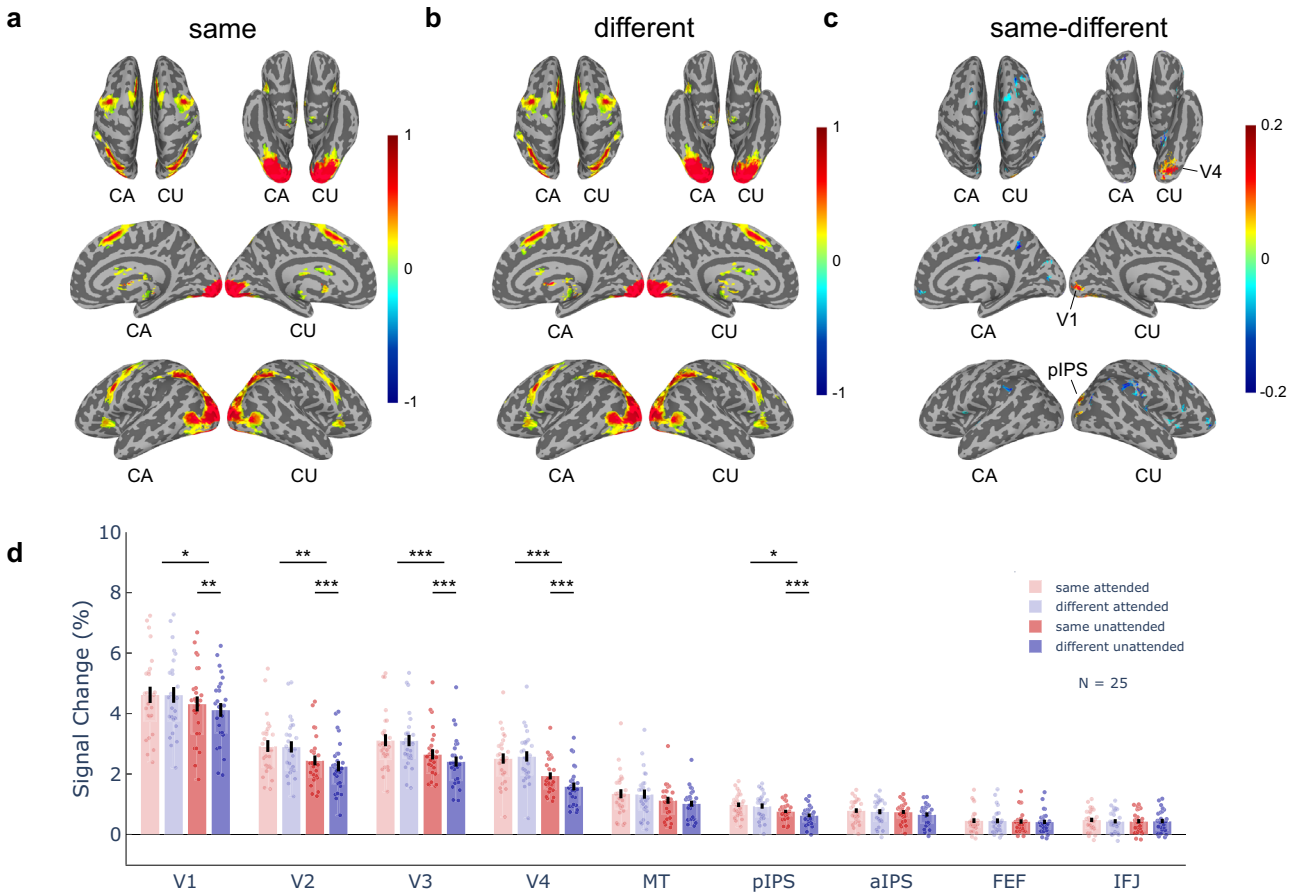

Fig. 5 | BOLD activation maps and spatially global effects of color-based attention in cortical regions. a–c are activation maps in same, different, and same-different conditions, respectively. $P < 0.05$, uncorrected. CA contralateral to the attended side, CU contralateral to the unattended side. **d** Bar plots in cortical ROIs. Error bars indicate SEM across participants. Short horizontal lines indicate significant differences between the "same" and "different" conditions; long horizontal lines denote significant interactions: $^{*}P < 0.05$, $^{**}P < 0.01$, $^{***}P < 0.001$, after Holm–Bonferroni correction. pIPS posterior IPS, aIPS anterior IPS, FEF frontal eye field, IFJ inferior frontal junction. Error bars represent SEM across participants ($n = 25$).

One interesting finding of the current study is that LGN activity in response to the attended stimulus was significantly reduced when the color of an unattended stimulus in the opposite visual field matched that of the attended stimulus (Fig. 2e). A similar trend was observed in the ventrolateral pulvinar (Fig. 4e). One possible explanation is that when the unattended stimulus shared the same color as the attended stimulus, a subcortical mechanism may automatically spread attention to and sample information from the opposite visual field, resulting in a slight reduction of thalamic response to the attended stimulus. This should reflect an increase in the scope of attention or a spatially global attentional sampling mechanism, rather than a shift of the attentional spotlight, since there was no significant difference in task performance or fixation eye movements between the same and different conditions (Supplementary Fig. S6). Furthermore, cortical regions did not exhibit a significant difference in responses to the attended stimulus between the two conditions (Fig. 5 and Supplementary Fig. S11), suggesting that the observed reduction in thalamic response arises from a subcortical mechanism. This effect is also unlikely due to a difference in eye movement, as this would have influenced both cortical and subcortical responses similarly.

Another key finding is that color-based attention significantly modulated BOLD signals in the deeper layers (Fig. 3f), but not in the superficial layers (Fig. 3e) of the SC. The superficial layers of the primate SC mainly process visuosensory information, while the intermediate and deep layers control attention and eye movement[47]. In a single-unit study in monkeys[55], neurons in the intermediate SC can respond strongly to isoluminant color stimuli, with a longer latency compared to luminance response, suggesting a cortical influence from frontoparietal attention networks[47,56]. In support of the cortical influence, the pattern of interaction effect in the SC is more similar to the cortical regions (Figs.3e and 5d). Thus, the SC may play a role in controlling the spatially global effect of feature-based attention. In support of with this claim, feature similarity between the attended and unattended stimuli across the visual field modulated the effective connectivity from the SC to the LGN (Fig. 6c, d), and the SC activity was also modulated by top-down connection from the IPS of parietal cortex (Fig. 6d). Although the global effect of color-based attention was not significant in the pulvinar (Fig. 4), effective connectivity analyses suggest that it might play a role in regulating information transmission between cortical regions in both attended and unattended locations across the visual field (Fig. 6). This finding suggests that the pulvino-cortical connections could serve as an important mechanism supporting the spatially global effect of feature-based attention.

In cortical regions, our results replicated the previous findings of spatially global effects of feature-based attention in the early- and intermediate-level visual cortices (Fig. 5)[9–13]. More importantly, we also found this effect in the posterior IPS of the parietal cortex. Effective connectivity analyses showed that top-down signals from the IPS significantly modulated activity in lower-level brain regions through the pulvinar and SC in feature-based attention across the visual field (Fig. 6d). Furthermore, attended color can be decoded from multivoxel response patterns in the contralateral IPS in both attended and unattended conditions (Fig. 7). These findings support an important role of the IPS in top-down control of the spatially global effect of feature-based attention. In the frontal regions

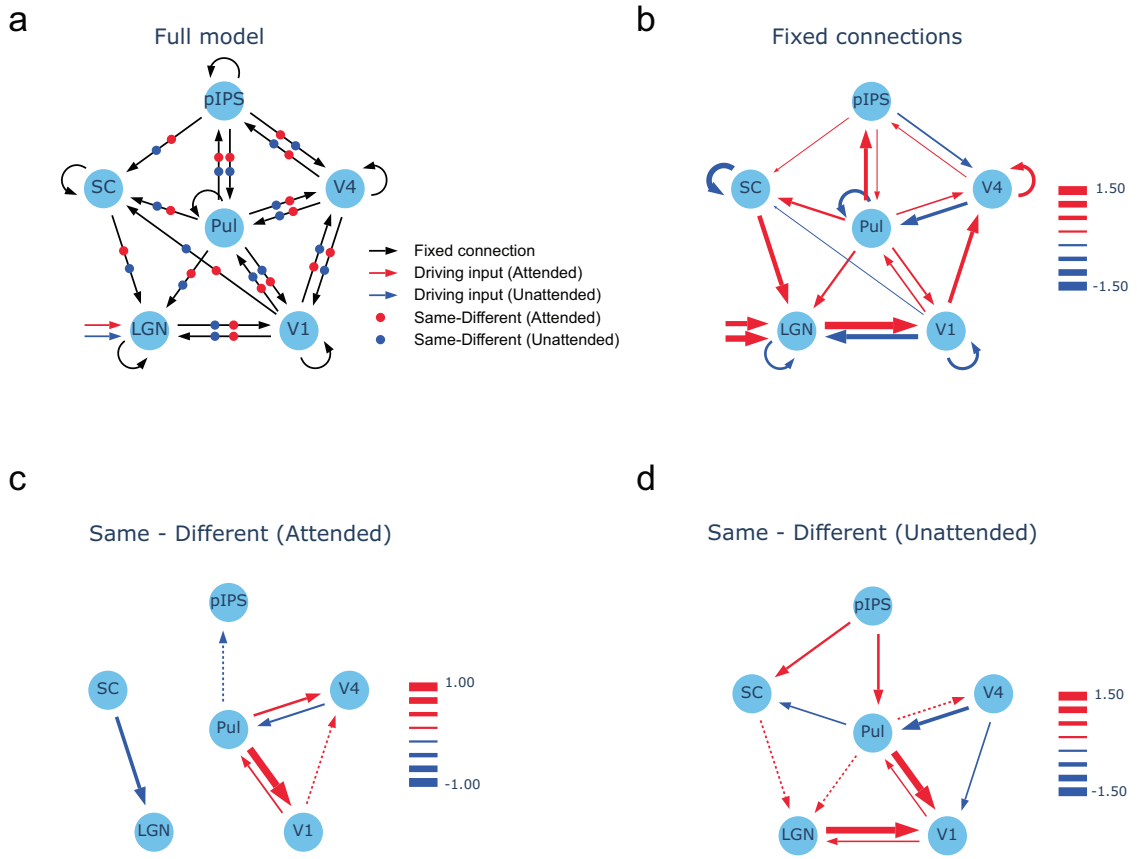

Fig. 6 | Dynamic causal modeling of effective connectivity in cortical and subcortical regions. a Shows the full DCM model. **b** Second-level results of fixed connections, including the driving inputs. **c**, **d** show the modulatory effect of feature similarity (same - diff) in attended and unattended conditions. Red and blue arrows in (**b**–**d**) denote positive and negative connections, respectively. Dotted and solid lines represent connections above 0.75 and 0.95 posterior probabilities, respectively. The scale bar of line width indicates the connectivity strength (Hz) averaged across participants ($n = 25$).

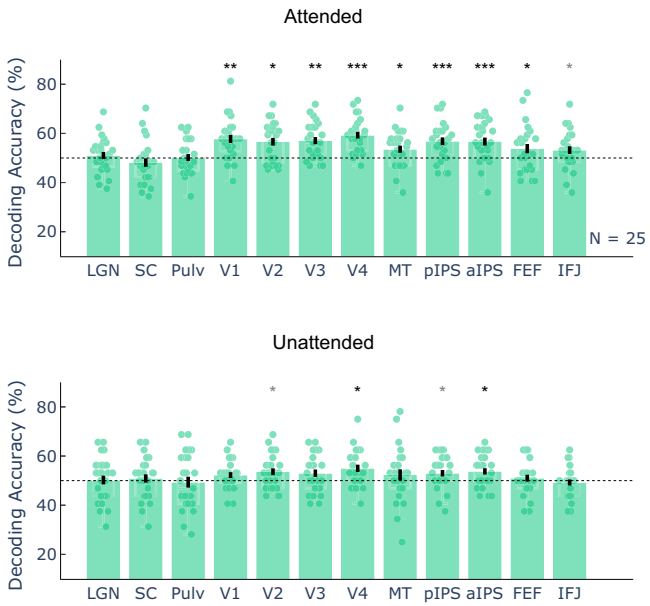

Fig. 7 | Decoding accuracy of attended color in brain regions contralateral to the attended and unattended locations. Top and bottom panels show the decoding accuracy of attended color in brain regions contralateral to the attended and unattended hemifields, respectively. Gray and Black asterisks indicate significance before and after correction for family-wise errors, respectively. $^{*}P < 0.05$, $^{**}P < 0.01$, $^{***}P < 0.001$. Error bars represent SEM across participants ($n = 25$).

(e.g., FEF, IFJ), attended color can be decoded from the contralateral hemisphere in the attended condition, consistent with a previous fMRI study at 3 T[14]. However, while another 3 T fMRI study showed enhanced frontal activity in the same compared to different conditions[13], we did not find this effect in our data (Fig. 5). One possible reason for this discrepancy is the difference in stimulus eccentricity. Due to the limited field of view of the head coil at 7 T, the eccentricity of our stimuli (4.25 degrees) is much smaller compared to the previous 3 T study (8.5 degrees). Given the large neuronal receptive field in frontal cortex, these regions might be more involved in controlling global feature-based attention in a larger field of view. Another possible reason is that, the spatial attention effect, i.e., the response difference between the attended and ignored sides, was only about half of the effect size in ref. 13. This may result in a larger baseline activity on the ignored side and a ceiling effect, making the modulation by feature-based attention between the same and different conditions less evident.

To summarize, our findings suggest distinct roles of subcortical nuclei in spatially global feature-based attention. The LGN of the thalamus serves as the earliest gatekeeper for processing the attended feature information, the deeper layers of the SC play roles in attentional control, and the ventral pulvinar regulates information transmission between visual areas. Interestingly and unexpectedly, our novel findings suggest a global attentional sampling mechanism by reducing the attended stimulus processing in the visual thalamus.

Methods

Participants

A total of 25 healthy human adults (15 females; 19–31 years of age) participated in this study. All participants had normal or corrected-to-normal

vision and reported no history of neuropsychological or vision disorders. The spatially global effects of feature-based attention showed a large effect size (d-prime >0.8) in cortical regions[10,13]. Due to the lower SNR in subcortical regions, the effect size was expected to be lower, thus we selected a sample size of 25 participants to provide 80% power to detect at least a medium effect size (d-prime = 0.5). Experimental protocols were approved by the Institutional Review Panel at the Institute of Biophysics, Chinese Academy of Sciences (Ethic No. 2012-IRB-011). Written informed consent was obtained from all participants prior to their participation in the study. All ethical regulations relevant to human research participants were followed.

Stimuli and procedures

Apparatus and calibrations. Visual stimuli were generated in MATLAB (Mathworks Inc.) with Psychtoolbox Version 3 (PTB-3)[57,58]. In the behavioral session, visual stimuli were presented by a LCD monitor at 1920 × 1080 pixels and 120-Hz refresh rate (Display + +, Cambridge Research System). In the fMRI session, stimuli were presented by an MRI-compatible LCD monitor at 1920 × 1080 pixels and 60 Hz refresh rate (BOLDscreen 3D, Cambridge Research System). Participants viewed the stimuli through a rear-view mirror mounted inside the head coil. Both displays were gamma corrected to achieve a linear luminance output with lookup tables. The red, green, and blue spectral power distributions were measured using a Photo Research PR-655 spectroradiometer (Chatsworth, CA, USA).

Behavioral experiment. Spatially overlapping red and green dot fields were presented in a circular region on each side of the fixation point at 4.5° eccentricity (Fig. 1a). The size of the dot fields was 5.5° in diameter. Dots were updated at random locations within the circular aperture every 33 ms. The chromaticity of the stimuli was defined in a three-dimensional cone contrast space[59,60]. In this space, cone contrasts represent the ratios of cone excitation levels within the same cone type. Therefore, using cone contrasts allows for control of visual inputs from the early stage of color processing, namely, the absorption of light by cones as a function of wavelength. We used a red-green stimulus that isolated L-/M-cone opponency by setting the activation weights of each cone to 1, -a, and 0, where a was the ratio of L- to M-cone weights for red-green (RG) isoluminance. To determine RG isoluminance, participants performed a minimum motion task[61] before the experiments by adjusting a counter-phase flickering horizontal grating until a minimum motion was perceived.

Participants performed two independent color discrimination tasks simultaneously on both visual fields. The magnitude of the red/green color contrast change was determined for each participant in a pilot experiment using a 3-down-1-up staircase procedure. In the beginning of each trial in the formal experiment, two colored dots were presented on each side of the fixation point to indicate the target dots to be attended in the following presentation. After pressing a button, spatially overlapping red/green dots were presented twice on both sides of the fixation point in two 1000-ms intervals, separated by 100-ms black background. Participants were instructed to respond in which interval the color of the target dots appeared more saturated. After responding to stimuli in both visual fields, feedback was given by a cross (wrong) or a checkmark (correct). The experiment consisted of four runs of cue combinations: red or green cues on both sides (same condition), left red/right green or left green/right red (different condition). Fifty trials were collected for each run, and a total of 100 trials were collected for the same or different conditions. The order of the four runs was randomized across participants.

fMRI localizer. The localizer stimuli were uniform red/green disks alternating at 2 Hz on each side of the fixation point against an equiluminant gray background, presented at the same size and location as those in the behavioral and fMRI experiments. The chromatic flickers were presented for 16 s in each stimulus block, followed by a 16-s fixation period. Each run lasted 272 s. Participants performed a simple fixation task, detecting occasional contractions of the fixation point. A total of two runs were scanned for each participant.

fMRI experiment 1. Red and green dot fields were identical to those used in the behavioral experiment. A black background was used to strongly activate both M and P layers of the LGN. Before the start of each run, participants were informed of the location of the stimulus to be attended by an arrow at the fixation point. Stimuli were presented in 20-s blocks, alternating with 12-s fixation blocks. From 2 s before the start of each stimulus block, the white fixation point turned red or green to indicate the target color to be attended to in the following presentation. Each stimulus block consisted of 8 trials. Spatially overlapping red and green dots were presented at the cued location, with a set of dots of either the same or different color as the attended dots, which were presented on the opposite side of fixation. The dots stimuli were presented twice in each trial, in two 833-ms intervals, separated by 83-ms fixation between the two presentations, followed by another 750-ms fixation before the next trial. Participants were required to maintain central fixation and indicate which interval contained a more saturated appearance of the attended color. In each stimulus block, both dot fields at the attended location could change color. Therefore, to perform the task accurately, participants needed to focus on the saturation change of the target color itself, rather than relying on the contrast between the two colors. Each run lasted 284 s. A total of four runs were collected for Exp. 1. The difficulty of the color discrimination task was adjusted to the threshold level by an adaptive staircase procedure during the structural scan.

fMRI experiment 2. Stimuli and procedures were identical to those in Exp. 1, except that spatially overlapping red and green dots were presented on both the attended and unattended sides of the fixation point. Four runs of data were also collected for Exp. 2.

MRI data acquisition

MRI data were collected on a 7 T scanner (Siemens Magnetom) with a 32-channel receive 1-channel transmit head coil (NOVA Medical). Functional data were collected with a T2*-weighted 2D GE-EPI sequence (1.5 mm isotropic voxels with 68 axial slices, FOV = 183 × 183 mm, TR = 2000 ms, TE = 22 ms, flip angle = 70°, phase partial Fourier = 6/8, GRAPPA = 2, multiband factor = 2, phase encoding direction from A to P). T1-weighted anatomical volumes were acquired with a MP2RAGE sequence (0.7 mm isotropic voxels, 256 sagittal slices, FOV = 224×224 mm, GRAPPA = 3, TR = 4000 ms, TE = 3.05 ms, TI1 = 750 ms, flip angle = 4°, TI2 = 2500 ms, flip angle = 5°, phase/slice partial Fourier = 7/8). A total of ten runs of fMRI data were scanned in the 7 T experiment, including two runs for the chromatic localizer, and four runs each for Exp. 1 and Exp. 2 (one participant finished 3 runs for Exp. 2 due to physical discomfort). The order of experimental conditions was counterbalanced across runs and participants. A bitebar was used to reduce head motion.

MRI data preprocessing

T1-weighted MP2RAGE anatomical images were segmented and reconstructed into gray matter and white matter surfaces in FreeSurfer (version 6.0)[62]. GE-EPI functional images were preprocessed by AFNI[63], advanced normalization tools (ANTs)[64], and custom Python code (https://github.com/herrlich10/mripy), in the following steps: slice timing correction, EPI distortion correction with nonlinear warping (Blip up/down method), rigid body motion correction, alignment of corrected EPI images to T1-weighted anatomical volume (cost function: lpc), upsampling by a factor of 2 to reduce the resolution loss caused by interpolation[38,65], and per run scaling as percent signal change. To minimize image blur, all spatial transformations and upsampling were combined and applied to the functional images in one interpolation step (sinc method). General linear models with a short time-to-peak HRF (Block4 in AFNI) were used to estimate BOLD signal change from baseline for each stimulus condition. Motion parameters were

included as regressors of no interest. The statistical results of subcortical regions were transformed into MNI space using a nonlinear mapping (antsRegistration) between the anatomical volume and the symmetric T1-weighted template from CIT168 atlas[66]. To improve the registration accuracy in subcortical regions, a spherical weight mask including the visual thalamus and the upper brainstem was used in the nonlinear warping process.

ROI definition and analysis

Anatomical ROI for subcortical regions were first defined on the high-resolution MNI template, and then manually edited for each individual based on their T1-weighted anatomical images in MNI space. With high T1 contrast at 7 T (Supplementary Fig. S13), the LGN appeared darker than the surrounding white matter and brighter than the cerebrospinal fluid in the ventricle, allowing its anatomical boundaries to be accurately defined by an experienced experimenter. Due to their proximity, the LGN and the ventral pulvinar of the thalamus were carefully delineated on the sagittal slices. To assist the group-level analysis, the coordinates of the left LGNs were mirror-flipped to the right, and then all LGNs were registered to the LGN of the MNI template by a 12-parameter linear (affine) transformation. SC and pulvinar ROIs were defined using the same procedure.

To analyze data from the functional subdivisions of the LGN, a normalized layer index was calculated for each voxel in the MNI template (Supplementary Fig. S1). Two layers of voxels were first defined, corresponding to the ventral and dorsal surfaces of the LGN. For the rest of the voxels, we calculated a layer index as the normalized distances to the dorsal and ventral surfaces (depth = 0 and 1 correspond to the dorsal and ventral surfaces, respectively). ROIs for the M and P subdivisions were determined from the layer index map according to the volume ratio of M/P layers of human LGNs (M/P volume ratio = 1/4)[45]. To generate the depth map of the SC (Supplementary Fig. S7), two layers of voxels were first defined from the superficial and deep surfaces of the SC. Then, a normalized depth map was calculated for each voxel as the ratio of shortest distances to the superficial and deep surfaces (depth = 0 and 1 correspond to superficial and deep surfaces, respectively). Based on the anatomy of the primate SC[47], the SC was split into a superficial and a deeper layer compartment at depth = 1/3. Pulvinar subdivisions were delineated based on task-co-activation patterns (Supplementary Fig. S8)[48], including the ventromedial (vmPul), ventrolateral (vlPul), dorsolateral (dlPul), dorsomedial (dmPul) and anterior (aPul) subdivisions of pulvinar. Since our stimuli mainly activated the ventral pulvinar (Fig. 4c), only data from vlPul and vmPul were used for the ROI-based analysis.

Cortical ROIs were defined on the inflated standard surface (std141 in AFNI). The early visual cortices V1, V2, V3, V4, and MT were defined based on the polar angle atlas from the 7 T retinotopic dataset of Human Connectome Project (Supplementary Fig. S9)[67,68]. Frontoparietal areas pIPS, aIPS, FEF, and IFJ were defined manually based on the anatomical landmarks and the group-level activations in the functional localizer (thresholded at $t > 0$, Supplementary Fig. S10). Volume ROIs were generated by transforming the surface ROIs to the volume space (3dSurf2Vol in AFNI).

For the analysis of ROI-averaged responses and timecourses in Exp. 1, 24 upsampled voxels (corresponding to the volume of three original voxels) that are most responsive to the chromatic localizer were selected from the P subdivision of the LGN, while the same number of voxels were selected from the M subdivision with the strongest activations to the attended dots on black background in Exp. 2. For the superficial and deep SC, voxels ($n = 24$) most responsive to the attended stimulus in Exp. 2 were selected from the ROIs. From vmPul and vlPul subdivisions, 100 voxels that are most responsive to the attended stimulus in Exp. 2 were selected. For the early visual cortices, voxels with significant activation to the chromatic localizer ($P < 0.05$ uncorrected) were used. All voxels were used in the frontoparietal ROIs.

The timecourses of LGN and pulvinar showed a clear transient response followed by a sustained phase (Figs. 2 and 4). to avoid the non-specific transient signals due to arousal change and transient attention[46], we focused on the sustained response in the analysis of ROI-averaged responses. The time window for the sustained response was defined from the "knee" point, marking the transition between the transient and sustained phases up to the stimulus offset. A leave-one-subject-out approach was employed to determine the sustained response time window based on the group-averaged time course. Different stimulus and attention conditions shared the same baseline for the time course analysis, which was estimated by a general linear model.

Attended color decoding

For both cortical and subcortical areas, we also trained linear support vector machine (SVM) classifiers[69] in the native space to decode the attended color (red or green) from multivoxel response patterns to stimulus blocks in ROIs contralateral or ipsilateral to the attended location, using a leave-one-run-out cross-validation procedure. Each stimulus block was modeled with a separate regressor in the GLM. For attended color decoding in cortical regions, feature selection was performed with K-1 runs of training data to select voxels with strong color-selective responses in the ROI (top 10% activated voxels in the chromatic localizer). Activation patterns were normalized by z-score across samples (or stimulus blocks). Given the limited number of voxels in subcortical ROIs, all voxels were used in this analysis. An SVM classifier was trained from K-1 runs of data, and the distance to the decision boundary was used to classify the attended color for each stimulus block from the remaining run. The cross-validation procedure was repeated for all runs, and the results were pooled together to calculate the decoding accuracy.

Color similarity (same vs. different) decoding

Since subcortical regions exhibit less variability in anatomy, we normalized the volumetric data of each subject in the MNI space, and trained linear support vector machines to predict whether a trial was from the "same" or "different" condition, using a leave-one-subject-out cross-validation (i.e., we trained on N-1 subjects, and tested on the unseen one, assuming that the difference in activity patterns between the two conditions was consistent across subjects). The analysis was performed separately for the subcortical ROIs contralateral to the attended or unattended side. Feature selection was done by choosing voxels with the largest activation difference between the two conditions, and the fraction was determined using a nested fourfold cross-validation within the training set. Each data sample was then pre-processed by dividing its L2-norm to remove the effect of the overall activation level difference. The test samples were first averaged by category to boost SNR before being fed to the classifier. The critical level for evaluating the significance of decoding accuracy corrected for multiple comparisons was obtained in a permutation procedure. The null distribution for the maximum mean decoding accuracy was constructed by randomly flipping the sign of the accuracy difference away from the chance level for each subject, taking the group mean, and finding the maximal value across conditions and ROIs. This was repeated 1000 times, and the accuracy at 5% was the critical value.

Dynamic causal modeling

Effective connectivity of fMRI data was analyzed using the DCM module of SPM12 (version 2020-Jan-13th). fMRI data were preprocessed in AFNI with slice timing and motion corrections. The mean timecourses of the LGN and SC were averaged from 24 upsampled voxels with the strongest similarity-by-attention interaction. The vlPul timecourses were averaged from 100 voxels with the strongest interaction effect. ROIs for the cortical regions were defined as voxels with a significant feature similarity effect (same-different $t > 1.96$) in the unattended condition. A full DCM model was defined based on the empirical evidence of anatomical connections among these brain regions (Fig. 6a). At the first level, the full DCM model was estimated for the fMRI data within each hemisphere for each individual, and the results were averaged between the two hemispheres using a Bayesian fixed effect (FFX) average (spm_dcm_average). At the second level, we used Bayesian model reduction, Bayesian model average, and parametric

empirical Bayes to make inference about the model evidence and connectivity strength (spm_dcm_peb and spm_dcm_peb_bmc).

Statistics and reproducibility

For the ROI-averaged responses, we performed repeated measures (rm) ANOVA with attention (attended/unattended), feature similarity (same/diff), and ROI as the fixed effects, and subjects (sample size = 25) as the random effect. Post-hoc paired t-tests were performed if there was a significant attention by similarity interaction. Based on the rationale of the seminal paper by Levin and colleagues[70], test of simple effects following a significant 2-by-2 interaction does not need further correction for family-wise errors. Holm–Bonferroni correction was used to control the family-wise error of the attention by similarity interaction effect across ROIs in Fig. 5d. A nonparametric permutation test was used to control the family-wise error of attended color decoding performance across ROIs (Fig. 7)[71]. In each permutation, the label of attended color was randomly shuffled within each run, and the entire cross-validation was applied, resulting a group mean accuracy for each ROI under null hypothesis. The permutation procedure was repeated 1000 times. A null distribution was generated by taking the maximum group-level accuracy across ROIs in each permutation. The family-wise error of the decoding performance in each ROI was derived from the null distribution. The behavioral experiment reproduced the findings of a previous study[43]. The spatially global effect in five cortical regions (V1/V2/V3/V4/IPS) reproduced the findings of previous fMRI studies[10,13].

Reporting summary

Further information on research design is available in the Nature Portfolio Reporting Summary linked to this article.

Data availability

Data to reproduce the main findings of this study can be downloaded from National Basic Science Data Center (https://www.scidb.cn/en/s/nIvyQn). Raw data can be requested by contacting the corresponding author P.Z. (zhangpeng@ibp.ac.cn).

Code availability

The mripy package, used in this study for high-resolution fMRI data processing, is available on GitHub (https://github.com/herrlich10/mripy).

Received: 10 December 2024; Accepted: 9 September 2025;
Published online: 15 October 2025

References

1. Liu, T. & Hou, Y. Global feature-based attention to orientation. *J. Vis.* **11**, 1–8 (2011).
2. White, A. L. & Carrasco, M. Feature-based attention involuntarily and simultaneously improves visual performance across locations. *J. Vis.* **11**, 1–10 (2011).
3. Scolari, M., Edward, F. & Serences, J. T. Feature- and object-based attentional modulation in the human visual system. *Oxf. Handb. Atten.* **573**, 600 (2014).
4. Carrasco, M. Visual attention: the past 25 years. *Vis. Res* **51**, 1484–1525 (2011).
5. Nobre, K. & Kastner, S. *The Oxford Handbook of Attention* (Oxford Library of Psychology, 2014).
6. Corbetta, M., Miezin, F. M., Dobmeyer, S., Shulman, G. L. & Petersen, S. E. Attentional modulation of neural processing of shape, color, and velocity in humans. *Science* **248**, 1556–1559 (1990).
7. Chawla, D., Rees, G. & Friston, K. J. The physiological basis of attentional modulation in extrastriate visual areas. *Nat. Neurosci.* **2**, 671–676 (1999).
8. Treue, S. & Martinez Trujillo, J. C. Feature-based attention influences motion processing gain in macaque visual cortex. *Nature* **399**, 575–579 (1999).
9. Martinez-Trujillo, J. C. & Treue, S. Feature-based attention increases the selectivity of population responses in primate visual cortex. *Curr. Biol.* **14**, 744–751 (2004).
10. Saenz, M., Buracas, G. T. & Boynton, G. M. Global effects of feature-based attention in human visual cortex. *Nat. Neurosci.* **5**, 631–632 (2002).
11. Serences, J. T. & Boynton, G. M. Feature-based attentional modulations in the absence of direct visual stimulation. *Neuron* **55**, 301–312 (2007).
12. Zhang, W. & Luck, S. J. Feature-based attention modulates feedforward visual processing. *Nat. Neurosci.* **12**, 24–25 (2009).
13. Zhang, X., Mlynaryk, N., Ahmed, S., Japee, S. & Ungerleider, L. G. The role of inferior frontal junction in controlling the spatially global effect of feature-based attention in human visual areas. *PLoS Biol.* **16**, e2005399 (2018).
14. Liu, T., Hospadaruk, L., Zhu, D. C. & Gardner, J. L. Feature-specific attentional priority signals in human cortex. *J. Neurosci.* **31**, 4484–4495 (2011).
15. Bichot, N. P., Heard, M. T., DeGennaro, E. M. & Desimone, R. A source for feature-based attention in the prefrontal cortex. *Neuron* **88**, 832–844 (2015).
16. Stalter, M., Westendorff, S. & Nieder, A. Article feature-based attention processes in primate prefrontal cortex do not rely on feature similarity ll Feature-based attention processes in primate prefrontal cortex do not rely on feature similarity. *Cell Rep.* **36**, 109470 (2021).
17. Saalmann, Y. B. & Kastner, S. Gain control in the visual thalamus during perception and cognition. *Curr. Opin. Neurobiol.* **19**, 408–414 (2009).
18. Halassa, M. M. & Kastner, S. Thalamic functions in distributed cognitive control. *Nat. Neurosci.* **20**, 1669–1679 (2017).
19. Saalmann, Y. B., Pinsk, M. A., Wang, L., Li, X. & Kastner, S. The pulvinar regulates information transmission between cortical areas based on attention demands. *Science* **337**, 753–756 (2012).
20. Krauzlis, R. J., Lovejoy, L. P. & Zénon, A. Superior colliculus and visual spatial attention. *Annu. Rev. Neurosci.* **36**, 165–182 (2013).
21. O'Connor, D. H., Fukui, M. M., Pinsk, M. A. & Kastner, S. Attention modulates responses in the human lateral geniculate nucleus. *Nat. Neurosci.* **5**, 1203–1209 (2002).
22. Schneider, K. A. & Kastner, S. Effects of sustained spatial attention in the human lateral geniculate nucleus and superior colliculus. *J. Neurosci.* **29**, 1784–1795 (2009).
23. McAlonan, K., Cavanaugh, J. & Wurtz, R. H. Guarding the gateway to cortex with attention in visual thalamus. *Nature* **456**, 391–394 (2008).
24. McAlonan, K., Cavanaugh, J. & Wurtz, R. H. Attentional modulation of thalamic reticular neurons. *J. Neurosci.* **26**, 4444–4450 (2006).
25. Petersen, S. E., Robinson, D. L. & Morris, J. D. Contributions of the pulvinar to visual spatial attention. *Neuropsychologia* **25**, 97–105 (1987).
26. Zhou, H., Schafer, R. J. & Desimone, R. Pulvinar-cortex interactions in vision and attention. *Neuron* **89**, 209–220 (2016).
27. Katyal, S., Zughni, S., Greene, C. & Ress, D. Topography of covert visual attention in human superior colliculus. *J. Neurophysiol.* **104**, 3074–3083 (2010).
28. Katyal, S. & Ress, D. Endogenous attention signals evoked by threshold contrast detection in human superior colliculus. *J. Neurosci.* **34**, 892–900 (2014).
29. White, B. J. et al. Superior colliculus neurons encode a visual saliency map during free viewing of natural dynamic video. *Nat. Commun.* **8**, 14263 (2017).
30. Schneider, K. A. Subcortical mechanisms of feature-based attention. *J. Neurosci.* **31**, 8643–8653 (2011).
31. Derrington, A. M. & Lennie, P. Spatial and temporal contrast sensitivities of neurones in lateral geniculate nucleus of macaque. *J. Physiol.* **357**, 219–240 (1984).

32. Derrington, A. M., Krauskopf, J. & Lennie, P. Chromatic mechanisms in lateral geniculate nucleus of macaque. *J. Physiol.* **357**, 241–265 (1984).
33. Felsten, G., Benevento, L. A. & Burman, D. Opponent-color responses in macaque extrageniculate visual pathways: the lateral pulvinar. *Brain Res* **288**, 363–367 (1983).
34. Casanova, C., Merabet, L., Desautels, A. & Minville, K. Higher-order motion processing in the pulvinar. *Prog. Brain Res.* **134**, 71–82 (2001).
35. Kaas, J. H. & Lyon, D. C. Pulvinar contributions to the dorsal and ventral streams of visual processing in primates. *Brain Res. Rev.* **55**, 285–296 (2007).
36. Arcaro, M. J., Pinsk, M. A. & Kastner, S. The anatomical and functional organization of the human visual pulvinar. *J. Neurosci.* **35**, 9848–9871 (2015).
37. Bridge, H., Leopold, D. A. & Bourne, J. A. Adaptive pulvinar circuitry supports visual cognition. *Trends Cogn. Sci.* **20**, 146–157 (2016).
38. Zhang, P., Zhou, H., Wen, W. & He, S. Layer-specific response properties of the human lateral geniculate nucleus and superior colliculus. *NeuroImage* **111**, 159–166 (2015).
39. Qian, Y. et al. Robust functional mapping of layer-selective responses in human lateral geniculate nucleus with high-resolution 7T fMRI. *Proc. Royal Soc. B: Biol. Sci.* **287**, 20200245 (2020).
40. Schneider, K. A., Richter, M. C. & Kastner, S. Retinotopic organization and functional subdivisions of the human lateral geniculate nucleus: a high-resolution functional magnetic resonance imaging study. *J. Neurosci.* **24**, 8975–8985 (2004).
41. Denison, R. N., Vu, A. T., Yacoub, E., Feinberg, D. A. & Silver, M. A. Functional mapping of the magnocellular and parvocellular subdivisions of human LGN. *Neuroimage* **102 Pt 2**, 358–369 (2014).
42. De Martino, F. et al. Spatial organization of frequency preference and selectivity in the human inferior colliculus. *Nat. Commun.* **4**, 1386 (2013).
43. Saenz, M., Buracas, G. T. & Boynton, G. M. Global feature-based attention for motion and color. *Vis. Res* **43**, 629–637 (2003).
44. Huang, L. & Pashler, H. A Boolean map theory of visual attention. *Psychol. Rev.* **114**, 599–631 (2007).
45. Andrews, T. J., Halpern, S. D. & Purves, D. Correlated size variations in human visual cortex, lateral geniculate nucleus, and optic tract. *J. Neurosci.* **17**, 2859–2868 (1997).
46. Saalmann, Y. B. & Kastner, S. Cognitive and perceptual functions of the visual thalamus. *Neuron* **71**, 209–223 (2011).
47. May, P. J. The mammalian superior colliculus: laminar structure and connections. *Neuroanat. Oculomot. Syst.* **151**, 321–378 (2006).
48. Barron, D. S., Eickhoff, S. B., Clos, M. & Fox, P. T. Human pulvinar functional organization and connectivity. *Hum. Brain Mapp.* **36**, 2417–2431 (2015).
49. Qian, C. et al. Hierarchical and fine-scale mechanisms of binocular rivalry for conscious perception. *bioRxiv 2023* **02**, 528110 (2023).
50. Arcaro, M. J., Pinsk, M. A., Chen, J. & Kastner, S. Organizing principles of pulvino-cortical functional coupling in humans. *Nat. Commun.* **9**, 5382 (2018).
51. Ghodrati, M., Khaligh-Razavi, S. M. & Lehky, S. R. Towards building a more complex view of the lateral geniculate nucleus: recent advances in understanding its role. *Prog. Neurobiol.* **156**, 214–255 (2017).
52. Shipp, S. The functional logic of cortico-pulvinar connections. *Philos. Trans. R. Soc. Lond. B Biol. Sci.* **358**, 1605–1624 (2003).
53. Zeidman, P. et al. A guide to group effective connectivity analysis, part 1: first level analysis with DCM for fMRI. *Neuroimage* **200**, 174–190 (2019).
54. Zeidman, P. et al. A guide to group effective connectivity analysis, part 2: second level analysis with PEB. *Neuroimage* **200**, 12–25 (2019).
55. White, B. J., Boehnke, S. E., Marino, R. A., Itti, L. & Munoz, D. P. Color-related signals in the primate superior colliculus. *J. Neurosci.* **29**, 12159–12166 (2009).
56. Leichnetz, G. R. & Goldberg, M. E. Higher centers concerned with eye movement and visual attention: cerebral cortex and thalamus. *Rev. Oculomot. Res.* **2**, 365–429 (1988).
57. Kleiner, M., Brainard, D. & Pelli, D. What's new in Psychtoolbox-3? *Perception* **36**, 1–16 (2007).
58. Brainard, D. H. The Psychophysics Toolbox. *Spat. Vis.* **10**, 433–436 (1997).
59. Cole, G. R., Hine, T. & McIlhagga, W. Detection mechanisms in L-, M-, and S-cone contrast space. *J. Opt. Soc. Am. A* **10**, 38 (1993).
60. Mullen, K. T., Dumoulin, S. O., McMahon, K. L., de Zubicaray, G. I. & Hess, R. F. Selectivity of human retinotopic visual cortex to S-cone-opponent, L/M-cone-opponent and achromatic stimulation. *Eur. J. Neurosci.* **25**, 491–502 (2007).
61. Anstis, S. & Cavanagh, P. A minimum motion technique for judging equiluminance. In *Colour vision: Physiology and psychophysics* (eds Mollon, J. D. & Sharpe, L. T.) 155–166 (Academic, New York, 1983).
62. Fischl, B. FreeSurfer. *Neuroimage* **62**, 774–781 (2012).
63. Cox, R. W. AFNI: software for analysis and visualization of functional magnetic resonance neuroimages. *Comput Biomed. Res* **29**, 162–173 (1996).
64. Avants, B. B. et al. A reproducible evaluation of ANTs similarity metric performance in brain image registration. *Neuroimage* **54**, 2033–2044 (2011).
65. Wang, J., Nasr, S., Roe, A. W. & Polimeni, J. R. Critical factors in achieving fine-scale functional MRI: removing sources of inadvertent spatial smoothing. *Hum. Brain Mapp.* **1**, 21 (2022).
66. Pauli, W. M., Nili, A. N. & Michael Tyszka, J. Data descriptor: a high-resolution probabilistic in vivo atlas of human subcortical brain nuclei. *Sci. Data* **5**, 1800632018 (2018).
67. Benson, N. C., Butt, O. H., Brainard, D. H. & Aguirre, G. K. Correction of distortion in flattened representations of the cortical surface allows prediction of V1-V3 functional organization from anatomy. *PLoS Comput. Biol.* **10**, (2014).
68. Benson, N. C. et al. The Human Connectome Project 7 Tesla retinotopy dataset: description and population receptive field analysis. *J. Vis.* **18**, 23 (2018).
69. Pedregosa, F. et al. Scikit-learn: machine learning in Python. *J. Mach. Learn. Res.* **12**, 2825–2830 (2011).
70. Levin, J. R., Serlin, R. C. & Seaman, M. A. A controlled, powerful multiple-comparison strategy for several situations. *Psychol. Bull.* **115**, 153 (1994).
71. Nichols, T. E. & Holmes, A. P. Nonparametric permutation tests for functional neuroimaging: a primer with examples. *Hum. Brain Mapp.* **25**, 1–25 (2001).

Acknowledgements

This study was supported by the Ministry of Science and Technology of China (https://en.most.gov.cn/) STI2030-Major Projects (2022ZD0211900 to P.Z., 2021ZD0204200 to C.Q., 2022ZD0204802 to F.F.), National Natural Science Foundation of China (https://www.nsfc.gov.cn/english/site_1/index.html, 31930053 to F.F., 32000787 to C.Q.), Youth Innovation Promotion Association CAS (https://english.cas.cn/, 2021089 to C.Q.).

Author contributions

P.Z. and F.F. conceived the study, P.Z. designed the experiments, W.L., C.Q., S.L., and P.Z. performed the experiments, W.L., C.Q., S.L., and P.Z. analyzed the data, C.Q., Y.Z., X.Z., and P.Z. contributed materials and analysis tools, W.L., C.Q., Y.Z., and P.Z. drafted the manuscript, W.L., C.Q., S.L., and P.Z. revised the manuscript.

Competing interests

The authors declare no competing interests.

Additional information

Supplementary information The online version contains supplementary material available at https://doi.org/10.1038/s42003-025-08871-6.

Correspondence and requests for materials should be addressed to Peng Zhang.

Peer review information *Communications Biology* thanks Jens-Max Hopf and the other, anonymous, reviewers for their contribution to the peer review of this work. Primary Handling Editor: Jasmine Pan. A peer review file is available.